Available online at www.sciencedirect.com

ScienceDirect

Procedia Structural Integrity 2 (2016) 2355–2366

Structural Integrity Procedia

www.elsevier.com/locate/procedia

21st European Conference on Fracture, ECF21, 20-24 June 2016, Catania, Italy

Static and dynamic response of titanium alloy produced by electron beam melting

Mirone G.[1], Barbagallo R.[1], Corallo D.[1], Di Bella S.[2]

[1]*University of Catania, V.le A. Doria 6, 95125 Catania – Italy*
[2]*MT Ortho Srl, Via fossa lupo sn, 95025 Aci Sant'Antonio (CT)*

Abstract

The suitability of Titanium alloys for many specialized applications requiring excellent performances at both static and dynamic strain rates, benefits of modern manufacturing technologies like the additive manufacturing, oriented toward the obtainment of complicated component shapes.
The EBM methodology for the production of Ti6Al4V components is based on the localized melting of alloy powders by way of guided electron beams scanning the powder volume by successive planar trajectories; for this reason, the whole production process may confer a certain degree of anisotropy to the components. The material behavior of the EBM alloy may be orientation-dependent in terms of stress-strain elastoplastic response as well as in terms of damage sensitivity and ductile fracture under given triaxiality histories.
The static and dynamic behavior of a sintered Ti6Al4V alloy is investigated here by way of quasistatic tension-torsion tests and dynamic tensile Hopkinson bar (SHTB) tests.
The outcome of the latter experiments, compared to similar tests results from the literature concerning Ti alloy obtained by classical metallurgical techniques, gives some indications about how the technological process may affect the final performance of the material and the component.

Peer-review under responsibility of the Scientific Committee of ECF21.

Keywords: Ti6Al4V, true curve, Strain rate

1. Introduction

The Ti6Al4V alloy, known also like F136, is by far the most used titanium alloy. In general, the titanium alloys have an austenitic α-phase stable at high temperatures and a martensitic β-phase stable at lower temperatures. The F136 is a mixed α+β alloy. Adding aluminium tends to stabilize the α-phase, while vanadium stabilizes the β-phase.
The Electron Beam Melting (EBM) process developed by Arcam allows for end products with complex structures

Peer review under responsibility of the Scientific Committee of ECF21.
10.1016/j.prostr.2016.06.295

and geometries that, in many cases, are impossible to obtain by foundry process and standard machining techniques. EBM is an advanced process in the Solid Free Form Fabrication Industry, which consists in the manufacture of components obtained directly from the CAD model. The basic idea of this technology is to get the final product building it layer by layer; the geometric information, obtained from the 3D model, is translated into the product by melting the metal powder using an electron beam. This process can be applied to different alloys. The speed of growth is about 60 cm^3/h and the thickness of the metal powder layers vary from 0.05 to 0.20 mm. After each melting process, a movable element passes through the entire surface positioning the new powder layer.
Table 1 shows the chemical composition of the powder used for producing Ti6Al4V alloy.

Table 1 Chemical composition of the powder used for the Ti6Al4V alloy

Arcam Ti6Al4V						
Al	6%	Fe	O	N	H	Ti
V	4%	0.03%	0.015%	0.01%	0.003%	Bil

In this work, Ti-alloy specimens obtained by the above technology are subjected to quasistatic tests in pure tension and pure torsion via a Zwick motor-driven machine with dual actuator capability, and to dynamic tension by a split Hopkinson tensile bar (SHTB) assisted by high speed camera for improved cross section measurements allowing the derivation of the true curves.

2. Experimental Campaign

In this work, a test program has been designed to investigate the behaviour of the EBM Ti6Al4V under different loading conditions. The specimens, all with the same shape (Fig. 1), were produced by the MT Ortho Srl by way of an Arcam Q10 machine using EBM technology, capable of melting successive metal layers perpendicularly to the specimen axis. The specimens have been tested under static tension, static torsion and dynamic tension, in order to investigate both the Lode Angle and the strain rate influences. In particular, five static tensile tests, three static torsion tests and two high strain rate tests have been carried out.

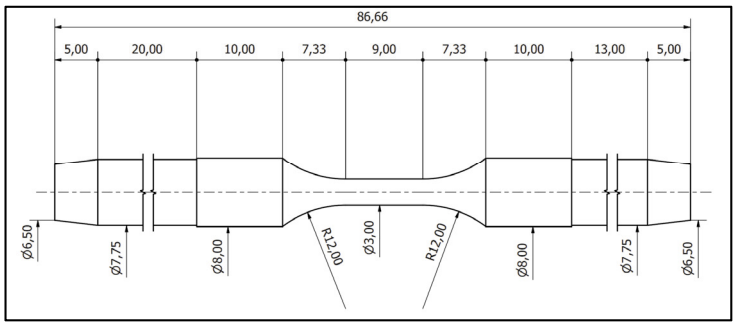

Fig. 1. Specimen geometry.

The static tensile and torsion tests have been performed using a Zwick/Roell Z100 machine, retrofitted with a torsional actuator and the respective control system, together with a camera recording for image acquisition and analysis (Fig. 2); instead the dynamic tests have been performed by way of a Split Hopkinson Tension Bar (SHTB) with fast camera recording (in Fig. 3 a frame captured at 150 000 fps).
The used production technology for the specimens has the drawback of generating specimens with a very high superficial roughness that can be only partially rectified with after production mechanical finishing. This characteristic causes a difficult post processing analysis of the camera images, especially in the dynamic tests where a lower resolution is essential for achieving high frame rates.
Moreover, the tolerance of about 0.2 mm and the ellipticity of the cross sections together with the small size of the specimens generates differences from the nominal diameter up to 6%.

Fig. 2. Static tensile test.

Fig. 3. Fast camera image of a dynamic tensile test.

3. Results

Fig. 4 shows the Force-Displacement curves of the tensile static tests extracted directly from the machine, showing a significant scattering of both maximum loads and displacements at fracture within the series of five specimens. The maximum load difference is due to the small differences in the diameter of the cylindrical segment, while the differences in elongation are reasonably due to the intrinsic characteristics of the material: the build-up process makes the material very irregular so it can contain little defects that can suddenly initiate the fracture.
The displacement readings of the machine are affected by the elastic deformation of the clamps so, elongation readings from camera images has been performed for getting the real elongation of the centre cylindrical segment of the scecimen. The corrected results are shown in Fig. 5.
The static torsion tests have been performed in “free end” modality, that is ideally without axial constrains on the specimen, in order to avoid axial forces and obtain a pure shear loading condition. In Figure 6 are shown the Moment-Rotation results of the static torsion tests extracted directly from the machine. Also in this case the maximum moment difference is due to the small differences in the gage length diameters while the different maximum displacement is reasonably due to the intrinsic sudden damage initiation of the material.
Also for the torsion tests, the elastic deformation of the clamps affects the rotation readings but, in this case, is not possible to use camera images analysis to correct them. Then, the curves have been corrected by subtracting an elastic torsion of the clamps estimated by imposing that torque and torsion at the first yield must agree with the elasticity modulus of the material assumed by literature. In Fig. 7 are shown the corrected curves.

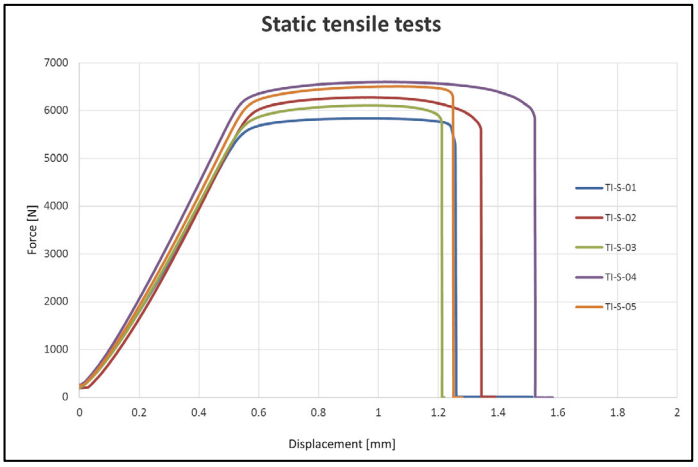

Fig. 4. Tensile tests, Force-Displacement results.

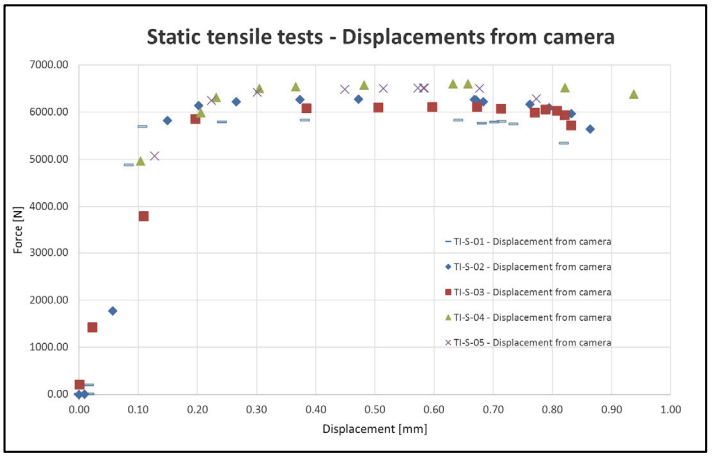

Fig. 5. Tensile tests, corrected Force-Displacement results.

While for the tensile tests, both static and dynamic, is it possible to obtain the true curves of the material synchronizing the camera images with the load curve of the machine and calculating the instant area of the necking section from the diameter extracted from the images, for the torsion tests a direct calibration procedure proposed by Nadai (Nadai, 1963) was used. Nadai's formulas allow to obtain the τ - γ curve directly from the Moment – Rotation experimental data:

$$\tau(\gamma_0) = \frac{1}{2\pi r_0^3}\left(\theta_n \frac{dM}{d\theta_n} + 3M\right) \quad , \quad \gamma_0 = \gamma(r_0) \tag{1}$$

Then it is possible to obtain the σ – ε curve considering the following well known correlations

$$\sigma_{eq} = \sqrt{3}\tau \quad , \quad \varepsilon_{eq} = \frac{\gamma}{\sqrt{3}} \tag{2}$$

Equations (1) and (2) can be applied directly to the experimental results but the obtained τ - γ curves (solid lines in Fig. 8) include a lot of noise because the derivative of the moment greatly amplifies the digital approximation of the torque measurement. Then, the same equations are applied successfully to the filtered experimental torque-torsion

data, leading to smooth τ - γ curves (dashed lines in Fig. 8).

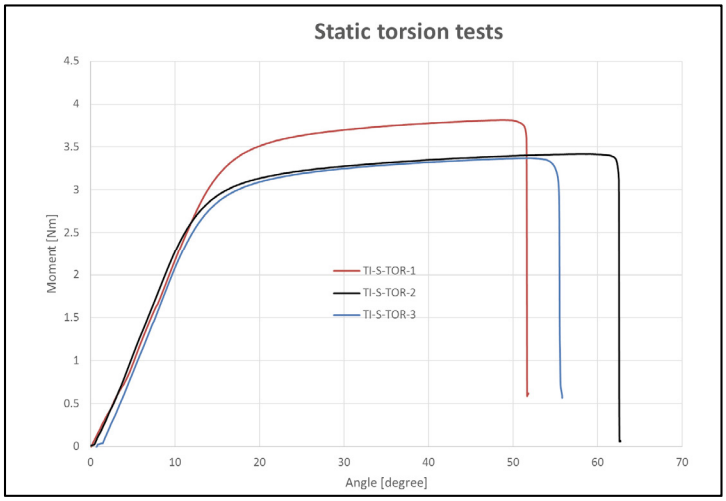

Fig. 6. Torsion tests, Moment-Rotation results.

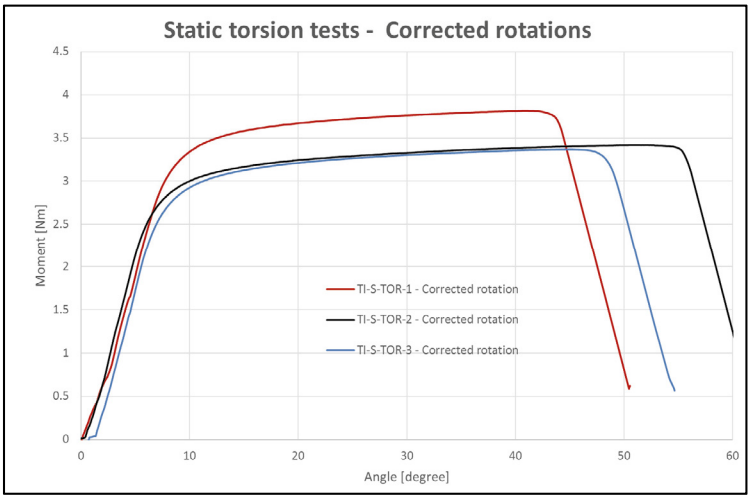

Fig. 7. Torsion tests, corrected Moment-Rotation results.

Fig. 9 shows the true curves obtained from the static tensile tests (circles), the static torsion tests (squares) and the dynamic tensile tests (triangles). The static tensile curves and the static torsion curves are very similar except for the deformation at fracture that is less than 0.05 for the torsion tests and around 0.20 for the tensile tests. Therefore, there is no lode angle influence on the stress-strain elastoplastic response but only in terms of damage sensitivity and ductile fracture.

There is also a clear strain rate influence, as the dynamic tests are significantly higher than the static ones (maximum dynamic tension around 1200 MPa while maximum static tension around 1080 MPa); however, in this case there is no influence on the deformation at fracture that is around 0.20 for both.

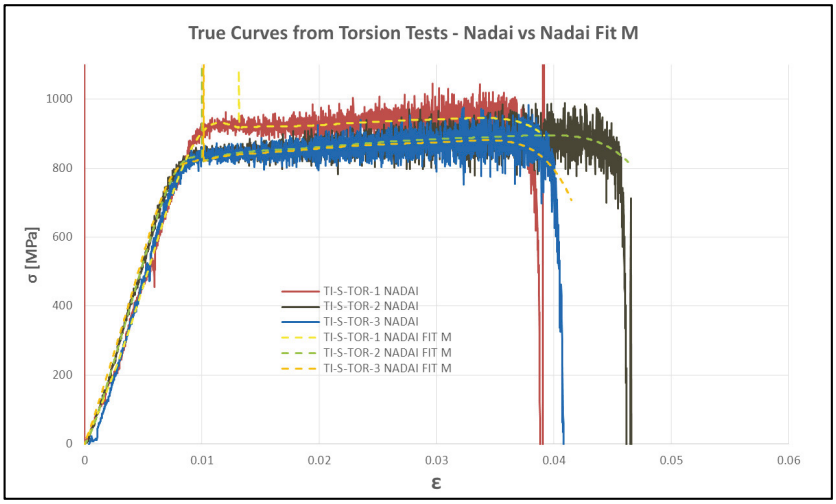

Fig. 8. Constitutive torsion curves, Nadai EXP vs Nadai FIT EXP.

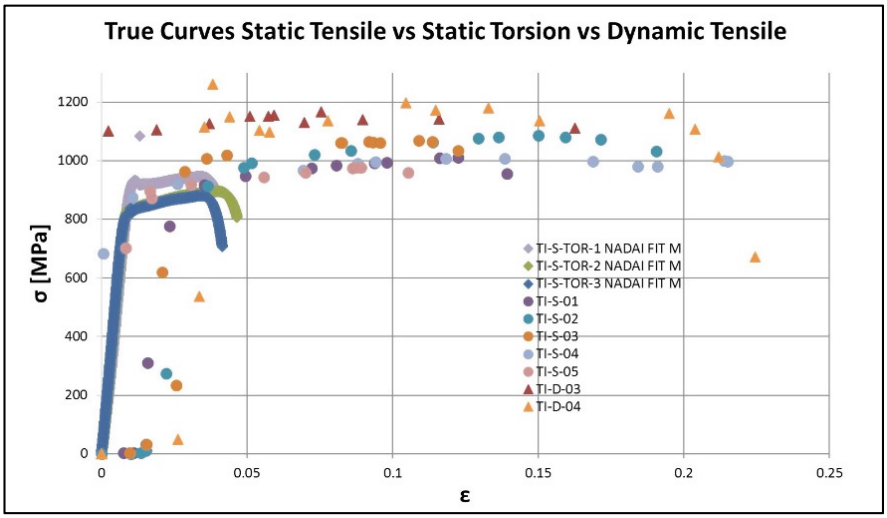

Fig. 9 True curves, Static Tensile vs Static Torsion vs Dy.

4. Material Model Calibration and Validatiom

Static calibration

The yield stress and the ε_{neck} of the *EMB Ti6Al4V* are calculated from the experimental data and shown in Table 2, while the elasticity modulus is assumed to be 110 GPa as widely suggested in the literature.

Table 2 EBM Ti6Al4V parameters

Yield Stress	ε_{neck}
790 MPa	0.075

The static true curves from tension and from torsion tests are approximated by the same power law reported in eq. 3 and plotted in Fig. 10

$$\sigma = 1230\ \varepsilon^{0.075} \tag{3}$$

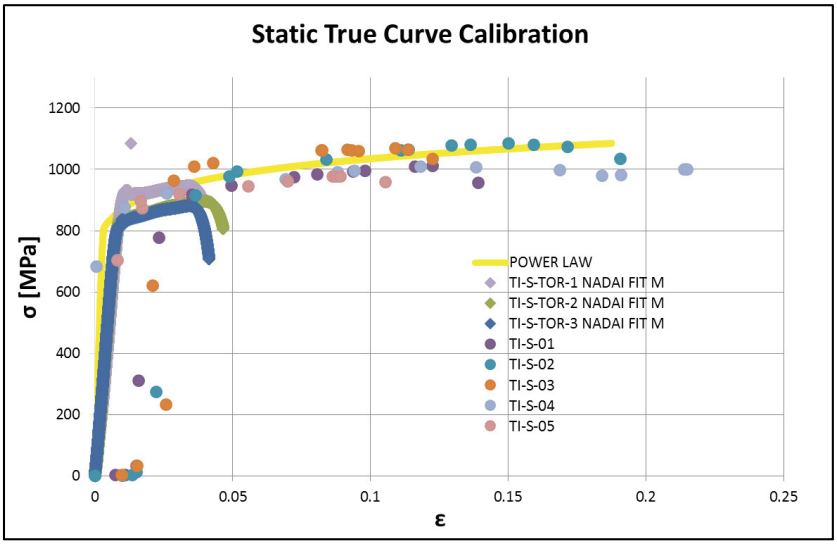

Fig. 10. Static true curves and fit.

The equivalent stress-strain curve from the torsion tests is identical to the true curve because this test is not affected by the necking. Instead the tensile test continue beyond necking before failure, so the corresponding equivalent stress-strain curve differs from the true curve, and can be found by the MLR function (Mirone, 2004). However for this Ti alloy, the deformation after necking is very small (from $\varepsilon_{neck} = 0.075$ to $\varepsilon_{failure} = 0.20$), thus the difference between the true curve and the equivalent curve is almost negligible as shown in Fig. 11.

FEM simulations have been made to validate the obtained material curves and, in particular, a 2D axisymmetric model to simulate the tensile test (Fig. 12a) and a brick 3D model to simulate the torsion test (Fig. 12b).

Fig. 11 shows, together with the obtained true and equivalent curves, the true curve regarding the FEM simulation in which σ is calculated as the total axial force divided by the instant area and ε is calculated from the instant area reduction.

The simulated true curve is almost identical to the desired bestfit curve marked by green triangles, although a considerable scattering affects the true stress-true strain data from experiments, as already discussed.

In Fig. 13, the Load-Displacement results of the tensile test simulation are compared to the corrected experimental data showing a very good agreement. Similarly, in Fig. 14, the Moment-Rotation results of the torsion test simulation are compared to the corrected experimental data; in this case, as was expected, the simulation curve stays in between the three different curves of the experiments.

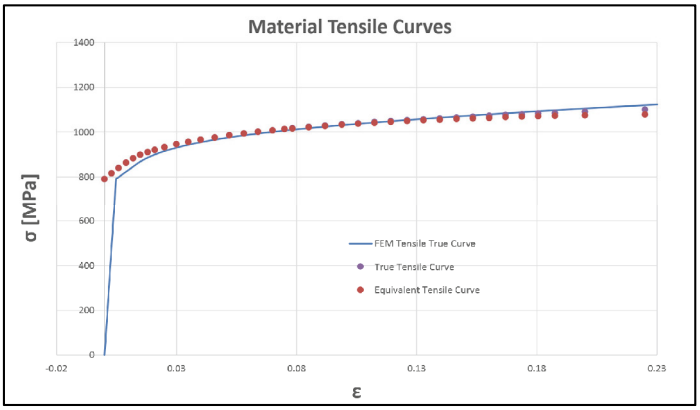

Fig. 11. True curve vs Equivalent curve vs FEM true curve.

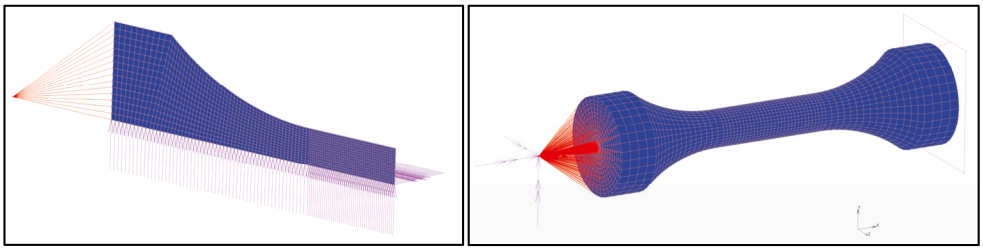

Fig. 12. a) Tensile axisymmetric FE model b) Torsion 3D FE model

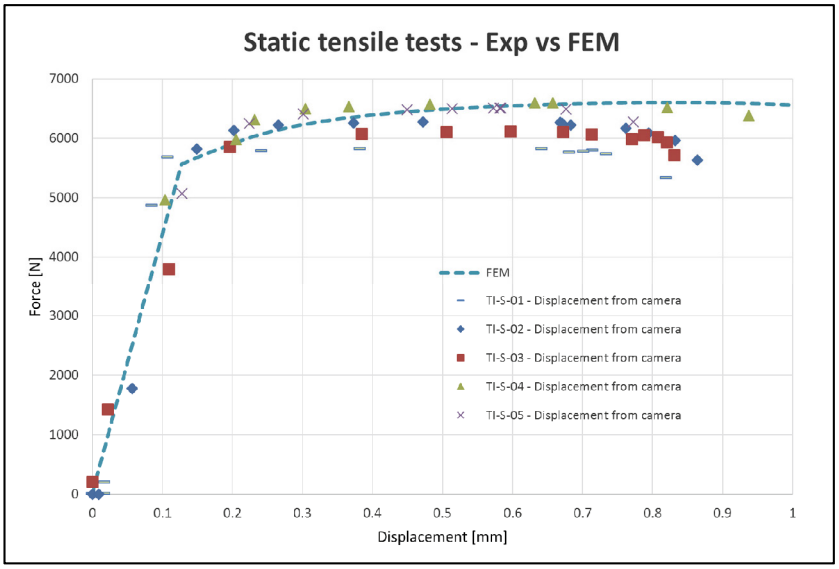

Fig. 13. Static tensile tests – Exp vs FEM.

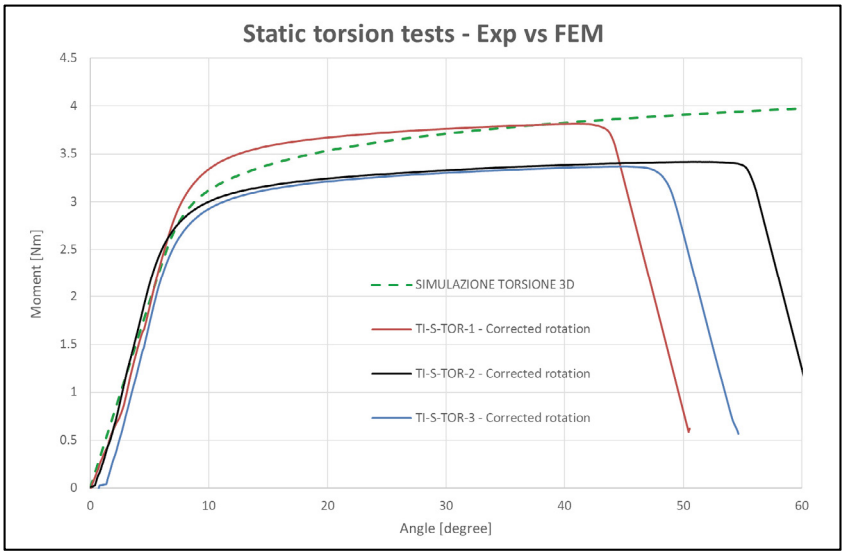

Fig. 14. Static torsion tests – Exp vs FEM.

Dynamic calibration

The dynamic true experimental data have been fitted with the following law representing an amplification of the static fitting law:

$$\varepsilon_{true} \leq \varepsilon_{true\_neck} \quad \rightarrow \quad \sigma = (k_0 + csr * \dot{\varepsilon}_{true})\, \varepsilon^{0.075} \tag{4}$$

$$\varepsilon_{true} > \varepsilon_{true\_neck} \quad \rightarrow \quad \sigma = (k_0 + csr * \dot{\varepsilon}_{true\_neck})\, \varepsilon^{0.075} \tag{5}$$

with

$k_0 = 1350$

$csr = 0.01$

$\dot{\varepsilon}_{true\_neck} = 1960\ s^{-1}$

This law reflects the fact that the amplification due to the strain rate is related to the actual strain rate value before the onset of necking while afterwards it is related only to the strain rate value at necking although the strain rate continues to increase after that. In Fig. 15 are shown the fitted dynamic true curve (solid line) together with the static true curve (dashed line) and the experimental dynamic data.

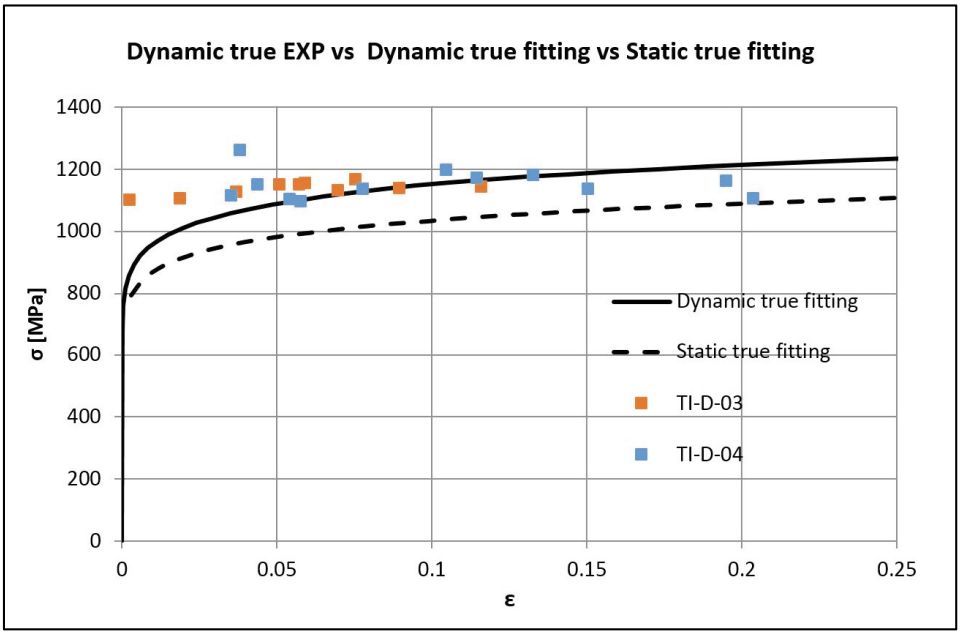

Fig. 15. Dynamic true EXP vs Dynamic true fitting vs Static true fitting.

Considering the strain rate $\dot{\varepsilon}_{true}$ corresponding to each point of the dynamic curve, it is possible to obtain the amplification ratio R_{true}, function of the strain rate, dividing the values of the true stress of the points of the dynamic curve by the values of the points of the static one with the same $\bar{\varepsilon}_{true}$

$$R_{true}(\dot{\varepsilon}_{true}) = \frac{\sigma_{truedyn_{\bar{\varepsilon}_{true}}}(\dot{\varepsilon}_{true})}{\sigma_{truestat_{\bar{\varepsilon}_{true}}}}$$

In Fig.16 it is shown the R_{true} together with the R, the ratio between the correspondent equivalent values, that is the same of the R_{true} until the strain rate at necking and afterwards it continues to increase linearly.

Implementing the obtained amplification law R, a dynamic transient simulation of the SHTB test has been made with a 2D axisymmetric FE model. In Fig. 17 the FEM true curve is compared to the dynamic fitting true curve and

to the experimental data showing a very good agreement. It is useful to underline that the simulation results are in accordance to the experimental data and to the fitted true dynamic curve also after the onset of necking despite the amplification law R implemented in the simulation was, after the strain rate at necking, greater than the Rtrue calculated directly from the fitted static and dynamic curves. This fact confirms that the behaviour of the material after the onset of necking is directly related to the strain rate history until the onset of necking and not to the actual strain rate.

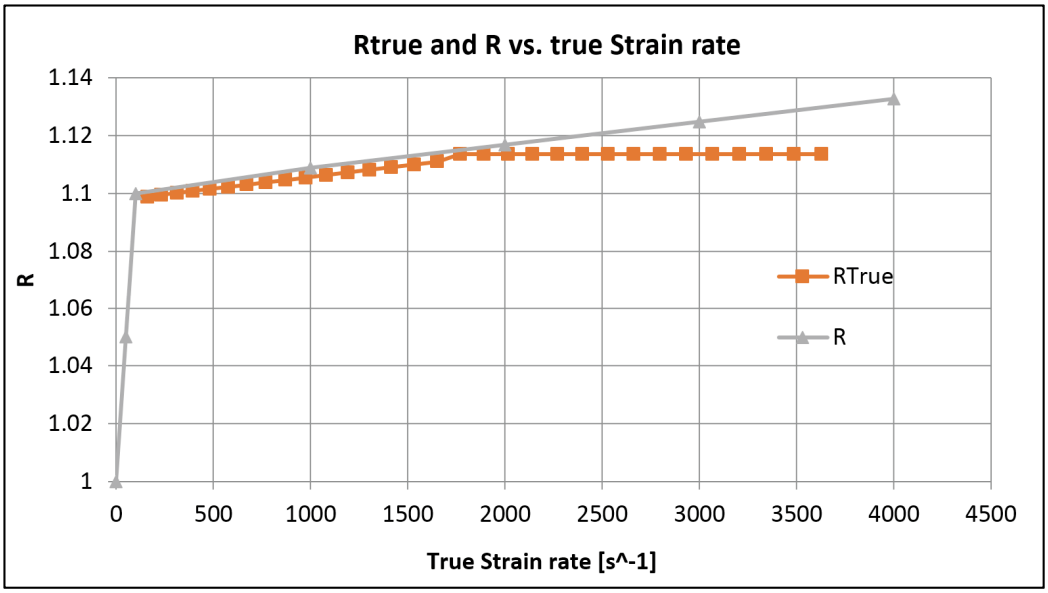

Fig.16. Rtrue and R vs true strain rate.

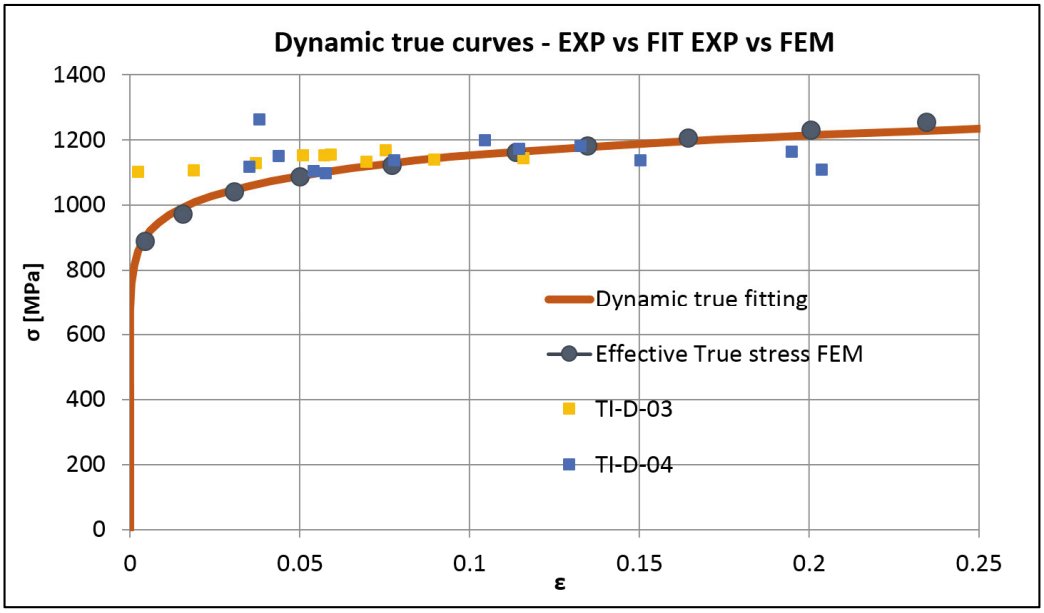

Fig. 17. Dynamic true curves – EXP vs FIT EXP vs FEM.

5. Comparison with literature data

The static and dynamic true curves obtained in this work from EBM Ti6Al4V specimens with axis orientation perpendicular to the melting plane (UNICT curves), are now compared to the following literature data:

- static and dynamic curves from rolled Ti6Al4V by Galàn et al. 2013, Peirs et al. 2011 (UGHENT curves),
- static curve from rolled Ti6Al4V by Allahverdizadeh et al. 2015 (POLIMI curves),
- static curves from EBM Ti6Al4V specimens with axis orientation parallel to the melting plane, by Rizza 2015 (UNICT-PW curves).

Fig. 18 shows the above comparison, reporting the static curves as dashed lines and the dynamic curves as solid lines.
The true static curves marked with "*" are obtained by transforming the engineering curves through the well-known relations $\sigma = S(1+e_p)$ and $\varepsilon = \ln(1+e_p)$, therefore they are reliable only until the onset of necking; after that point, a linear extension tangent to the curve (dotted part) is added, as a reasonably approximate prosecution of the true curve.

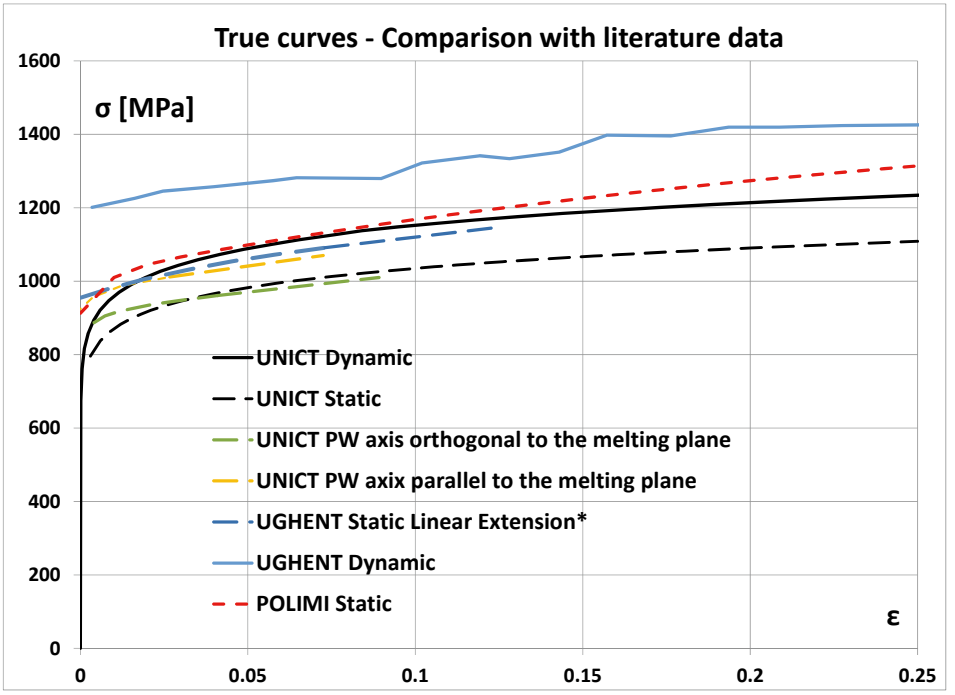

Fig. 18. True curves – Comparison with literature data. *Obtained from engineering curves, therefore after necking they are not reliable due to non-uniform strain

The orientation of the EBM specimens with respect to the melting plane of the machine has a great effect on the material behaviour.
When the axis of EBM specimens is parallel to the melting plane (UNICT-PW), the static response of the alloy is very similar that of the rolled alloy Ti-6Al-4V tested at the UGHENT and at the POLIMI. On the other hand, the specimens with axis perpendicular to the melting sections tested by Rizza, exhibit a static behaviour very similar to the initial response of the static specimen tested within this work, unless that the former curves are derived from the engineering curves then only extend up to strains of about 0.1, while the latter ones extend up to failure at more than twice the above strain.
All this data clearly shows that the axis orientation perpendicular to the melting plane decreases the static stress response of about 10% with respect to the case when the axix is parallel to the melting plane.

Similarly, the dynamic true curve obtained in this work is lower than the dynamic curve obtained at the UGHENT for the rolled Ti-6Al-4V; in this case the difference is also greater than it is for the static curves.

6. Conclusions

In this work the static and dynamic behaviour of EBM Ti6Al4V alloy is investigated by way of quasistatic tension-torsion tests and of dynamic tensile Hopkinson bar tests. True curves have been obtained directly from load readings and images analysis for static and dynamic tensile tests while a direct calibration procedure proposed by Nadai is used to extract the stress-strain data from torsion tests.
The obtained static torsion and tension curves are very similar except for the deformation at fracture; therefore, there is no Lode angle influence on the stress-strain elastoplastic response, although such effect shows up in terms of damage sensitivity and ductile fracture strain. Both tensile and torsion static FEM simulations show good agreement with experimental results.
The dynamic true experimental results are fitted with a law taking into account the fact that the amplification due to the strain rate is related to the actual strain rate value before the onset of necking while afterwards it is related only to the strain rate value at necking although the strain rate continues to increase after that point.
The strain rate-induced amplification R of the flow stress is modelled as a linear function which before necking coincides with the RTrue ratio, while after necking the RTrue becomes almost constant and R continues monotonically according to the same linear function and the two curves depart each other.
The above voluntary spoiling of the RTrue produces a simulated true curve exactly identical to the desired fitting of the experimental true curves.
This fact confirms that the strain rate amplifies the true curve of the material only until necking which is already postulated in other papers.
The obtained static and dynamic true curves are compared to data from the literature showing the influence of the specimen orientation inside the EBM machine on the material behaviour, and the differences with the rolled alloy with the same chemical composition.
It is found that EBM specimens obtained by melting sections parallel to the specimen axis have comparable behaviour to the rolled specimens; on the contrary, specimens with their axis perpendicular to the melting plane present lower true curves, of about 10% at quasistatic rates, and of about 15% at dynamic ones.

References:

Nadai, A., 1963. Theory of flow and fracture solids - 2. McGraw Hill, New York

Mirone, G., 2004. A new model for the elastoplastic characterization and the stress–strain determination on the necking section of a tensile specimen. Int. J. Solids Struct. 5 (41), 3545–3564.

Galàn J., Verleysen P., Degrieck J., 2013. Thermal Effects During Tensile Deformation of Ti-6Al-4V at Different Strain Rates, Strain – an international Journal for Experimental Mechanics 49(4), 354–365.

Peirs, J., Verleysen, P., Van Paepegem, W., Degrieck, J., (2011). Determining the stress-strain behaviour at large strains from high strain rate tensile and shear experiments, International Journal of Impact Engineering 38, 406-415.

Allahverdizadeh, N., Gilioli, A., Manes, A., Giglio, M. (2015), An experimental and numerical study for the damage characterization of aTi–6AL–4V titanium alloy, International Journal of Mechanical Sciences, 93, 32–47.

Rizza, F., (2015). Analisi numerica di una protesi di bacino custom made, Master Thesis, Mechanical Engineering, Department of Industrial Engineering, University of Catania.